$\pi^- p \to \pi^-\pi^+\pi^- p$ Reaction at 6 GeV/c†

K. F. Galloway, J. E. Mott, E. D. Alyea, Jr., K. Y. Lee,* H. J. Martin, and W. F. Prickett‡
Indiana University, Bloomington, Indiana 47401
(Received 31 December 1969)

This report is based on the study of 2300 events representing the $\pi^-\pi^+\pi^- p$ final state produced by the interactions of 5.97-GeV/c π^- mesons with protons in the Argonne National Laboratory 30-in. hydrogen bubble chamber. This final state has a cross section of 1.39±0.15 mb and is dominated by ρ^0 production (0.60±0.08 mb) and $\Delta^{++}(1236)$ production (0.39±0.06 mb). There is evidence for the production of A_1 and $A_{1.5}$ mesons in the 3π mass spectrum in addition to the A_2. Some characteristics of the $\pi\rho p$ and $\pi\pi\Delta$ final states can be explained with a double-Regge-exchange model.

I. INTRODUCTION

DURING the past few years, the $\pi^- p \to \pi^-\pi^+\pi^- p$ reaction has been studied by several experimental groups.[1–3] Abundant production of ρ^0 and $\Delta^{++}(1236)$ generally characterizes this final state. Three-particle resonances, such as the A_2 meson and higher isobars, have also been observed. Data on this reaction at 6 GeV/c are presented and analyzed in this paper.

II. EXPERIMENTAL DETAILS

The data for the experiment were obtained from a 96 000-picture exposure in the Argonne National Laboratory 30-in. hydrogen bubble chamber. The beam momentum was 5.97±0.05 GeV/c.

The film was scanned twice for four-prong events occurring within a restricted fiducial volume. 19 840 events were found, measured on image-plane and film-plane digitizers, and geometrically reconstructed with TVGP. 92% of the events passed the reconstruction.

In order to categorize the four-prong events into different reactions, ionization tests were first imposed. Events where both positive tracks were definitely not protons were eliminated from the sample. Those events with a definite proton or at least one positive track which could possibly be a proton were examined for consistency with one of the following reactions:

$$\pi^- p \to \pi^-\pi^+\pi^- p \quad (1)$$

$$\to \pi^-\pi^+\pi^- p + n\pi^0, \quad n \geq 1. \quad (2)$$

A scattergram of missing energy (W_{miss}) versus missing momentum (P_{miss}) calculated in the lab system was plotted assuming reaction (1). Reaction-(1) events should have $W_{\text{miss}} = P_{\text{miss}} = 0$. However, the measuring errors will lead to a distribution of points about the origin. Figure 1 shows the scattergram for ~15% of the events passing the initial ionization tests. Some events, in which both positive tracks passed the ionization criteria, appear twice. The events clustered at the origin and along the lines where $|W_{\text{miss}}| = P_{\text{miss}}$ should belong to reaction (1); events inside the dashed line were selected as the initial sample. The events which cluster about the solid line intercepting the W_{miss} axis at 0.1396 GeV represent reaction (2) with $n = 1$. A detailed account of this method of event selection has been published.[4]

The initial sample, selected as described above, was submitted to two additional tests. First, positive tracks with a proton assignment were reexamined for ionization consistency on the scanning table if their momentum lay between 0.8 and 1.5 GeV/c. Second, a χ^2 test for energy-momentum conservation was imposed; a χ^2 cutoff at 20 was made for the $\pi^-\pi^+\pi^- p$ final state.

The selection criteria yielded 2300 events repre-

† Research supported in part by the National Science Foundation.

* Present address: National Accelerator Laboratory, Batavia, Ill.

‡ Present address: University of Manitoba, Winnipeg, Manitoba, Canada.

[1] 1.0–4.5 GeV/c: Saclay-Orsay-Bari-Bologna Collaboration, Nuovo Cimento **29**, 515 (1963); R. Christian, A. R. Erwin, H. R. Fechter, F. E. Schwamb, S. H. Vegors, and W. D. Walker, Phys. Rev. **143**, 1105 (1966); D. D. Carmony, F. Grard, R. T. Van de Walle, and Nguyen-Huu Xuong, in *Proceedings of the 1962 Annual International Conference on High-Energy Nuclear Physics* (CERN, Geneva, 1962), p. 44; P. H. Satterblom, W. D. Walker, and A. R. Erwin, Phys. Rev. **134**, B207 (1964); P. R. Klein, R. J. Sahni, A. Z. Kovacs, and G. W. Tautfest, *ibid.* **150**, 1123 (1966); J. Alitti, J. P. Baton, A. Berthelot, B. Deler, W. J. Fickinger, N. Neveu-René, V. Alles-Borelli, R. Gessarolli, A. Romano, and P. Waloschek, Nuovo Cimento **35**, 1 (1965); A. W. Key, J. D. Prentice, N. R. Steenberg, E. West, T. S. Yoon, W. A. Cooper, W. Manner, L. Voyvodic, and W. D. Walker, Phys. Rev. **166**, 1430 (1968); S. U. Chung, O. I. Dahl, J. Kirz, and D. H. Miller, *ibid.* **165**, 1491 (1968); Y. Y. Lee, W. D. C. Moebs, B. P. Roe, D. Sinclair, and J. C. Vander Velde, *ibid.* **159**, 1156 (1967); Aachen-Birmingham-Bonn-Hamburg-London (I.C.)-München Collaboration, Nuovo Cimento **31**, 485 (1964).

[2] 4.5–8.0 GeV/c: B. Terreault, Ph.D. thesis, University of Illinois, 1969 (unpublished); S. Miyashita, J. von Krogh, J. B. Kopelman, and L. M. Libby, Phys. Rev. D **1**, 771 (1970); V. E. Barnes, W. B. Fowler, K. W. Lai, S. Orenstein, D. Radojičić, M. S. Webster, A. H. Bachman, P. Baumel, and R. M. Lea, Phys. Rev. Letters **16**, 41 (1966); N. M. Cason, Phys. Rev. **148**, 1282 (1966).

[3] 8.0–20.0 GeV/c: J. W. Lamsa, N. M. Cason, N. N. Biswas, I. Derado, T. H. Groves, V. P. Kenney, J. A. Poirier, and W. D. Shephard, Phys. Rev. **166**, 1395 (1968); N. N. Biswas, I. Derado, N. Schmitz, and W. D. Shephard, *ibid.* **134**, B901 (1964); C. Caso, G. Tomasini, P. Dittman, G. Drews, P. Von Handel, H. Nagel, L. Mandelli, S. Ratti, V. Russo, G. Vegni, P. Daronian, A. Daudin, C. Kochowski, and C. Lewin, Nuovo Cimento **47A**, 675 (1967); G. W. Brandenburg, A. E. Brenner, M. L. Ioffredo, W. H. Johnson, Jr., J. K. Kim, M. E. Law, J. E. Mueller, B. M. Salzberg, J. H. Scharenguivel, L. K. Sisterson, and J. J. Szymanski, Nucl. Phys. **B16**, 287 (1970); J. Ballam, A. D. Brody, G. B. Chadwick, D. Fries, Z. G. T. Guiragossián, W. B. Johnson, R. R. Larsen, D. W. G. S. Leith, F. Martin, M. Perl, E. Pickup, and T. H. Tan, Phys. Rev. Letters **21**, 934 (1968).

[4] H. J. Martin, Nucl. Instr. Methods **64**, 185 (1968).

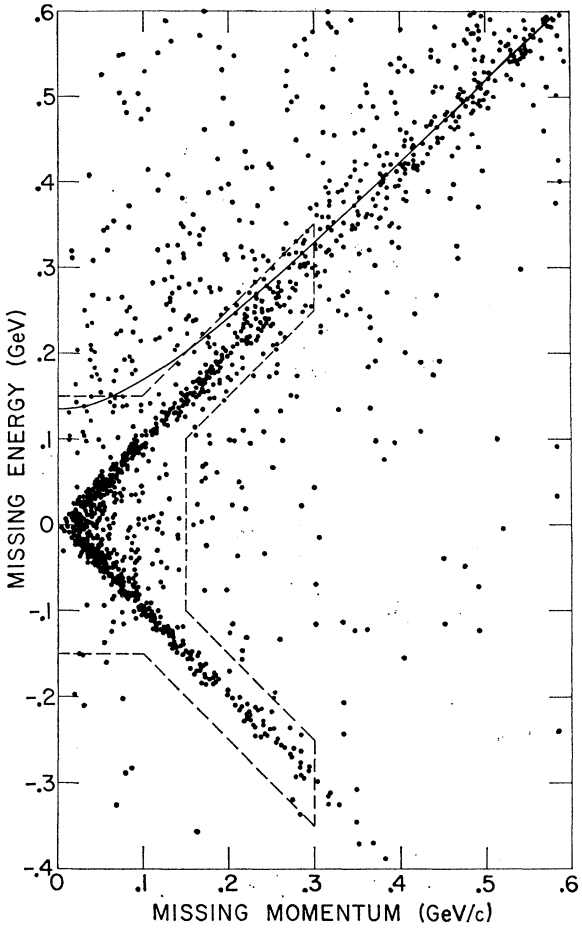

FIG. 1. Scattergram of missing momentum versus missing energy for four-prong events having a possible proton. The dashed curve represents the acceptance region for possible $\pi^-\pi^+\pi^-p$ events. The solid curve represents the line along which $\pi^-\pi^+\pi^-p\pi^0$ events would lie if there were no measuring errors.

senting the $\pi^-\pi^+\pi^-p$ final state. Of these events, 48 cases passed all tests with either positive track designated as the proton. Track assignments for these events were made on the basis of χ^2. Figure 2 shows the distribution of missing mass squared for the final sample. We estimate that non-$\pi^-\pi^+\pi^-p$ events account for less than 2% of the sample.

III. GENERAL FEATURES OF $\pi^-\pi^+\pi^-p$ FINAL STATE

A. Cross Sections

A total of 95 268 measurable pictures with an average of 16.8±0.2 beam tracks per picture were examined for four-prong events. The average beam flight path in the fiducial volume was 39.5±2.0 cm. The scanning efficiency was (95.1±0.6)%, and the measuring efficiency after remeasurements and after removing events with high film-measuring errors was (81.1±0.3)%. A study of the unassigned events indicated that about 170±50 true $\pi^-\pi^+\pi^-p$ were rejected by our selection criteria. After these corrections, the 2300 events corresponded to a yield of 1.65±0.11 events per μb.

The total cross section for $\pi^-p \rightarrow \pi^-\pi^+\pi^-p$ as measured in this experiment is 1.39±0.15 mb. Table I gives the cross sections for ρ^0 and $\Delta(1236)$ production. Figure 3 summarizes the variation with beam momentum of the total and partial cross sections.

B. Production Distributions

Figure 4 shows the production angular distributions in the center-of-momentum system of the initial particles. The backward peaking of the proton and the forward peaking of the π^- meson is typical of this reaction. If the two negative pions are separated on the basis of relative momentum transfer, we see a sharp forward peak for the low-momentum-transfer pion and an approximately isotropic distribution for the remaining pion [see shaded area in Fig. 4(c)].

Scatterplots of longitudinal momentum versus transverse momentum in the center-of-momentum system (Peyrou plots) for the three different final-state particles are displayed in Fig. 5. The tendency of the proton to continue in the same direction with only a small change in momentum can easily be seen. The "double-wing" structure of the π^+ distribution is due to the production of ρ^0 mesons and Δ^{++} isobars, the forward wing being primarily associated with the ρ^0 and the backward wing with the isobar.

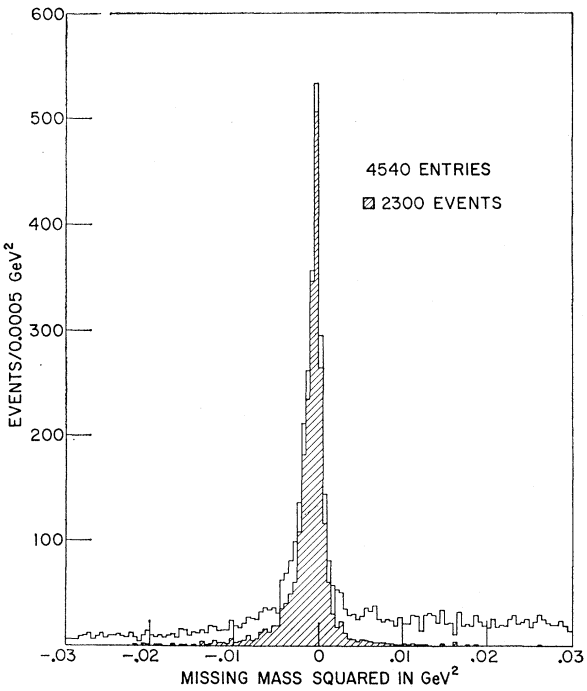

FIG. 2. Missing mass squared for all four-prong events with a possible proton. Shaded events represent the selected sample of $\pi^-\pi^+\pi^-p$ events.

TABLE I. Measured cross sections.

Final state	Events	Cross section (mb)
$\pi^-\pi^+\pi^- p$	2300± 70	1.39±0.15
$\pi^-\pi^-\Delta^{++}(1236)$	651± 80	0.39±0.06
$\pi^-\pi^+\Delta^0(1236)$	67± 17	0.04±0.01
$\pi^- p\rho^0$	990±115	0.60±0.08

IV. TWO-PARTICLE RESONANCE STATES

A. Δ^{++} Production

Figure 6(a) shows the $\pi^+ p$ effective mass distribution. The $\Delta^{++}(1236)$ production dominates this distribution. The solid curve on this figure represents a fit of the following function to the mass distribution:

$$F(M_R,\Gamma_R,f)=\left[(1-f)+\frac{fN\Gamma_R}{(M_E^2-M_R^2)^2+\Gamma_R^2 M_R^2}\right]f_{\rm PS}.$$

In this expression, M_R and Γ_R are the mass and width of the resonance; M_E is the effective mass of a $\pi^+ p$ combination; f is the fraction of events in which the resonance is produced; N is the normalization factor; and $f_{\rm PS}$ is the relevant phase-space factor. The resulting values for the mass and width should be interpreted as characteristic of the experimental distribution rather than as intrinsic values, since energy dependence of the width has not been accounted for. The fit gave the following values:

$$\begin{aligned}&\text{percentage } \Delta^{++} = (28\pm4)\%,\\ &\text{mass} = 1220\pm6 \text{ MeV},\\ &\text{width} = 94\pm7 \text{ MeV}.\end{aligned}$$

Figure 6(b) is the Chew-Low plot for the $\pi^+ p$ combination. The momentum-transfer variable plotted (t') is the difference between $|t|$, the absolute value of the four-momentum transfer squared from the target proton to the $\pi^+ p$ system, and $|t|_{\rm min}$, the minimum value possible for that particular $\pi^+ p$ effective mass. The variable t' is used throughout this paper. The peripheral

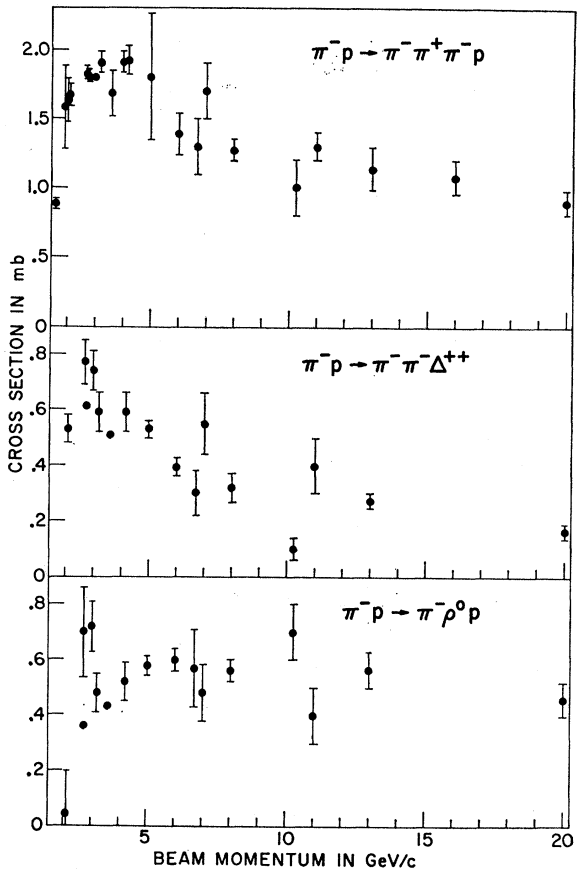

FIG. 3. Variation with incident lab momentum of the total and partial cross sections for the $\pi^- p \to \pi^-\pi^+\pi^- p$ reaction.

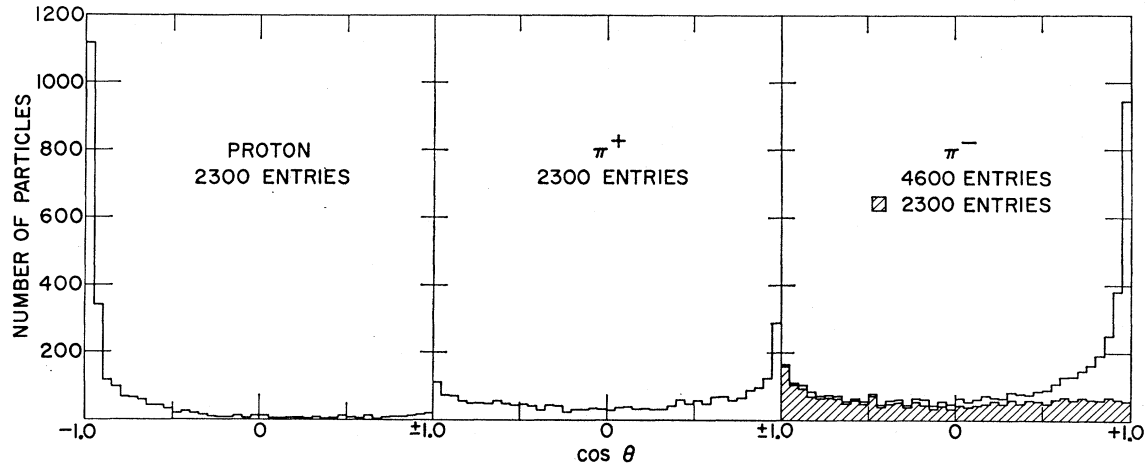

FIG. 4. Production center-of-momentum angular distributions for the particles in the $\pi^-\pi^+\pi^- p$ final state. The shaded area in the π^- distribution represents the π^- with the higher momentum transfer.

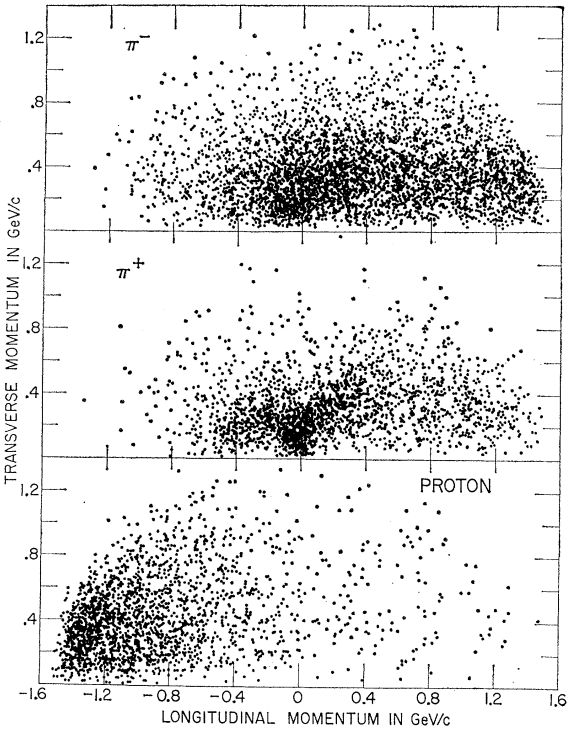

FIG. 5. Longitudinal versus transverse momentum in the overall center-of-momentum system for the particles in the $\pi^-\pi^+\pi^-p$ final state.

nature of the Δ^{++} production is evident. The events with $t'<1.0$ $(\mathrm{GeV}/c)^2$ are shown as the shaded curve in Fig. 6(a).

The events in the Δ^{++} region are defined by $1.15 \leq M(\pi^+p) \leq 1.33$ GeV,[5] and the decay angle in the Δ^{++} rest frame, defined as the angle between the decay p and incident p, is shown in Fig. 7(a). With this distribution normalized to unity, a fit to a power series in $\cos\theta$ keeping terms through $\cos^2\theta$, yields $I(\cos\theta)=0.32+0.30\cos\theta+0.54\cos^2\theta$. This is similar to the distribution $I(\cos\theta)=0.286+0.644\cos^2\theta$ which is observed for π^+p elastic scattering when the center-of-momentum energy is equal to the $\Delta^{++}(1236)$ mass,[6] and indicates that a single-pion-exchange mechanism might be responsible for the $\pi^-\pi^-\Delta^{++}$ final state. However the Treiman-Yang angle for the π^+p system exhibited in Fig. 7(b) shows an anisotropy. This could be consistent with pion exchange if absorption effects were taken into account[7] or might suggest some mechanism other than single-pion exchange such as Reggeized-pion exchange[8] as discussed in Secs. V A and V C.

[5] Throughout this paper the Δ^{++} band will be defined by $1.15 \leq M(\pi^+p) \leq 1.33$ GeV and the ρ^0 band by $0.65 \leq M(\pi^+\pi^-) \leq 0.85$ GeV.

[6] G. Källén, *Elementary Particle Physics* (Addison-Wesley, Reading, Mass., 1964), p. 86.

[7] K. Gottfried and J. D. Jackson, Nuovo Cimento **34**, 735 (1964).

[8] E. L. Berger, Phys. Rev. **179**, 1567 (1969).

B. ϱ^0 Production

In addition to the strong $\Delta^{++}(1236)$ signal, an even stronger ρ^0 signal is observed. Figure 8(a) shows the $\pi^+\pi^-$ effective mass. The solid curve represents a fit to the data using a form similar to Eq. (3). The phase-space factor was peripheralized using the production characteristics of the final-state proton.[9] The results of the fit are

$$\begin{aligned} &\text{percentage } \rho^0 = (43\pm5)\%, \\ &\text{mass} \qquad\quad = 765\pm6 \text{ MeV}, \\ &\text{width} \qquad\quad = 120\pm7 \text{ MeV}. \end{aligned}$$

The Chew-Low plot for the $\pi^+\pi^-$ combinations is shown in Fig. 8(b). An accumulation of low-t' combinations is noticeable in the ρ^0 region.

The Treiman-Yang angle is plotted in Fig. 7(d) for the $\pi^+\pi^-$ combinations in the ρ^0 band defined as $0.65 \leq M(\pi^+\pi^-) \leq 0.85$ GeV.[5] The distribution of the cosine of the scattering angle between the incident π^- and the outgoing π^- in the $\pi^+\pi^-$ rest frame is given in Fig. 7(c). The shaded events in Figs. 7(c) and 7(d) are $\pi^+\pi^-$

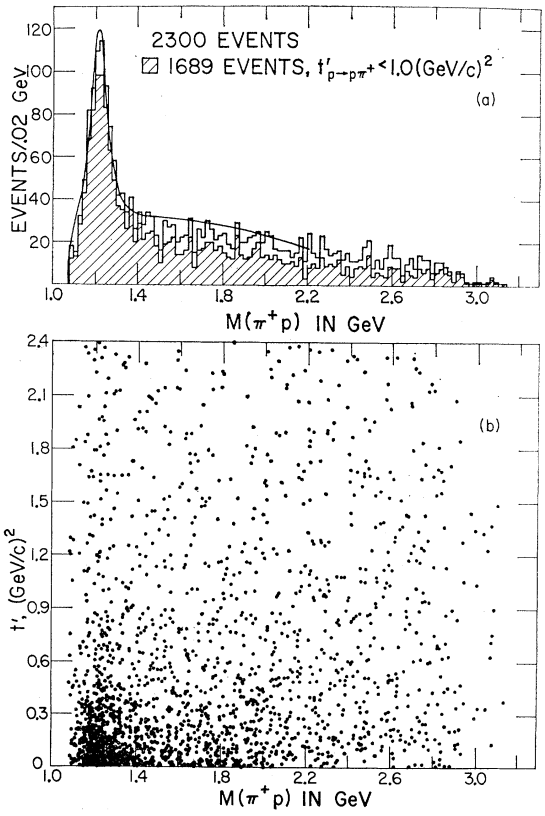

FIG. 6. (a) Effective-mass spectrum of the π^+p system. Shaded events have $t'\leq1.0$ $(\mathrm{GeV}/c)^2$. (b) Chew-Low plot for the π^+p system.

[9] T. Hofmokl, L. Michejda, S. Otwinowski, R. Sosnowski, M. Szeptycka, W. Wójcik, and A. Wróblewski, Nucl. Phys. **B4**, 573 (1968).

combinations falling in the ρ^0 band and having $t' < 1.0$ (GeV/c)^2. These events are also shaded in Fig. 8.

The ρ^0 mesons observed in this final state can be the decay products of mesons seen in the 3π mass spectrum or baryons having $\pi\pi N$ decays. They could also be produced in conjunction with a $\Delta^0(1236)$. These possibilities will be discussed in the following sections.

C. Neutral Isobar Production

Figure 9(a) shows the $\pi^- p$ invariant-mass spectrum. There is production of the $\Delta^0(1236)$ and some production of isobars in the 1500- and 1700-MeV mass regions.

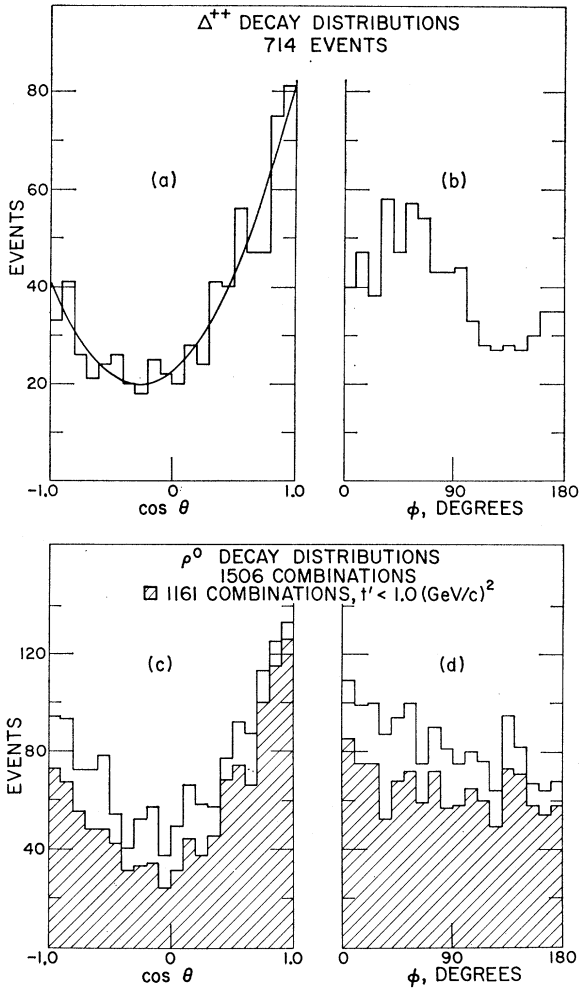

FIG. 7. (a) Cosine of the scattering angle of the π^+ in the Δ^{++} system defined as the polar angle of the π^+ in the $\pi^+ p$ rest system where the z axis is the direction of the target proton, the y axis is normal to the production plane, and the x axis completes a right-handed coordinate system. The solid curve is discussed in the text. (b) The Treiman-Yang angle of the π^+ in the Δ^{++} system defined as the azimuthal angle of the π^+ in the above system. (c) Cosine of the scattering angle for the π^- in the ρ^0 system. The definition is similar to the above except that the z axis is now the incident π^- direction in the $\pi^+\pi^-$ rest system. (d) Treiman-Yang angle for the π^- in the ρ^0 system.

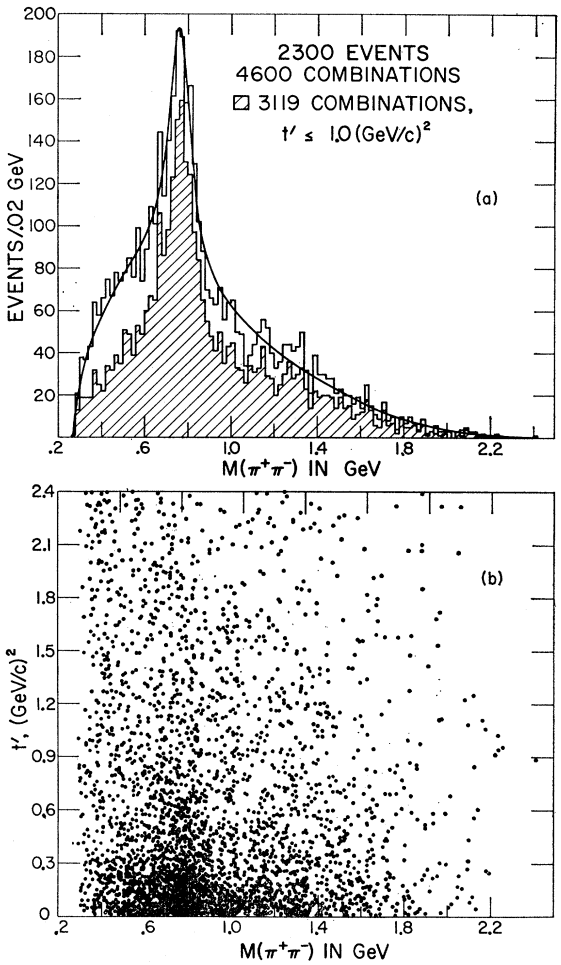

FIG. 8. (a) Effective-mass spectrum of the $\pi^+\pi^-$ system. Shaded events have $t' \leq 1.0$ (GeV/c)^2. (b) Chew-Low plot for the $\pi^+\pi^-$ system.

In general, the neutral isobars are weakly produced in the $\pi^- p \to \pi^-\pi^+\pi^- p$ reaction in this energy region. The number of events containing a $\Delta^0(1236)$ was estimated as 67 ± 17 by drawing a smooth curve through the data to estimate the background. The Chew-Low plot [t' versus $M(\pi^- p)$] is shown in Fig. 9(b). The $\pi^- p$ combinations with $t' < 1.0$ (GeV/c)^2 are shown as the shaded curve in Fig. 9(a). This t' cut does not diminish the Δ^0 signal and enhances the $N^*(1518)$. We estimate 55 ± 15 events in the $N^*(1518)$ peak corresponding to a cross section of 34 ± 10 μb.

The possibility of production of the quasi-two-body final state, $\pi^- p \to \rho^0\Delta^0(1236)$, was examined. A histogram of the $\pi_2^- p$ mass when the $\pi_1^-\pi^+$ mass lay within the ρ^0 band (not shown) gave no evidence for associated production.

D. $\pi^-\pi^-$ Production

The $\pi^-\pi^-$ mass is exhibited in Fig. 10 and shows no evidence for resonance production as would be expected, since there are no confirmed isospin-two-resonance

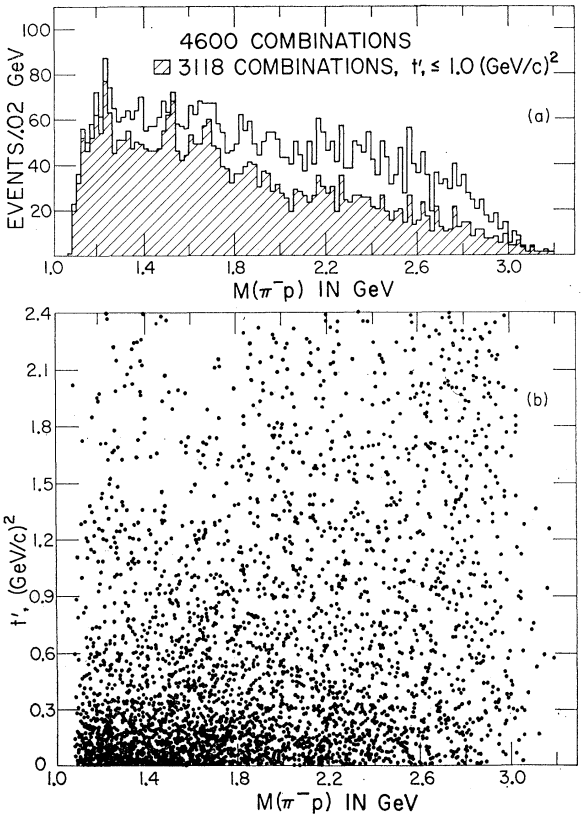

FIG. 9. (a) Effective-mass spectrum of the $\pi^- p$ system. Shaded events have $t' \leq 1.0$ (GeV/c)^2. (b) Chew-Low plot for the $\pi^- p$ system.

states. The $\pi^-\pi^-$ can be produced with a Δ^{++}. The shaded curve in Fig. 10 represents those events which have a $\pi^+ p$ combination in the $\Delta^{++}(1236)$ band. The decay angles for the $\pi^-\pi^-$ system in the $\pi^-\pi^-\Delta^{++}$ final state have been described by diffraction production combined with one-pion exchange and by double-Regge-trajectory exchange,[10] with the double-Regge-pole model (DRPM) giving the better description. An analysis of the $\pi^-\pi^-\Delta^{++}$ final state is discussed in Sec. V C.

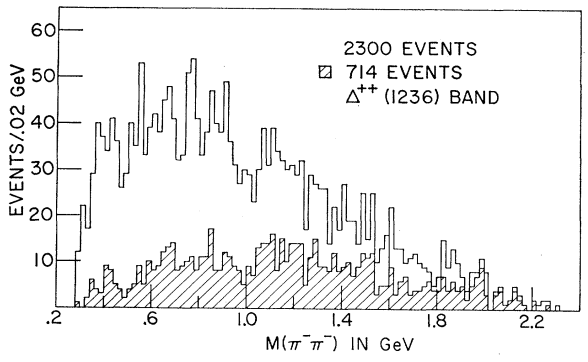

FIG. 10. Effective-mass spectrum of the $\pi^-\pi^-$ system. Shaded events are those with a $\pi^+ p$ combination in the $\Delta^{++}(1236)$ band.

[10] J. E. Mott, H. J. Martin, and K. F. Galloway, Nucl. Phys. **B16**, 102 (1970).

V. THREE-PARTICLE RESONANCE STATES

A. $\pi^+\pi^-\pi^-$ Mass Spectrum: *A* Mesons

A considerable amount of experimental work has been reported on the three-pion mass spectrum from the $\pi^- p \to \pi^-\pi^+\pi^- p$ reaction. The A_2 meson at 1300 MeV is firmly established in this reaction, and evidence far the splitting of this state (or two distinct states neor this mass) is mounting.[11] The A_1 meson near 1060 MeV is often explained as a kinematic effect. However, the appearance of the A_1 in several reactions where a simple kinematic effect cannot account for its presence tends to confirm its existence.[12] There are also indications of a narrow resonance lying between the A_1 and A_2 called the $A_{1.5}$.[13] Above the A_2 region, there is good evidence for a meson with a three-pion decay mode near 1650 MeV.[14] This state is often referred to as the A_3.

Figure 11(a) shows the effective mass of the $\pi^+\pi^-\pi^-$ system. Signals from the A_1 and A_2 mesons are apparent and there is some evidence for the $A_{1.5}$ near 1200 MeV. There is no evidence for production of the A_3.

All three of the states below 1400 MeV have been reported to have $\rho\pi$ decay modes. In this mass region, the ρ bands occupy a large fraction of the three-pion Dalitz plot and it is difficult to distinguish between the 3π and $\rho\pi$ decay modes of these states. The shaded histogram in Fig. 11(a), representing the $\rho\pi$ mass spectrum, was obtained by requiring that at least one of the $\pi^+\pi^-$ combinations lie in the ρ^0 band. Figure 8(a) shows that this ρ^0 cut contains a sizable number of non-ρ^0 events. We estimate that we obtain $\sim$730 true $\rho\pi$ combinations and $\sim$540 non-$\rho\pi$ combinations by making this ρ^0 mass cut.

The Chew-Low plot for the $\pi^+\pi^-\pi^-$ system is shown in Fig. 11(b). The peripheral nature of the events below 1400 MeV is evident. The extreme peripheral nature of the A_1 region is illustrated in Fig. 12. The events contributing to the A_1 and $A_{1.5}$ enhancements are primarily those events that have $t' < 0.1$ (GeV/c)^2.

The low-mass $\rho\pi$ enhancement predicted by the Deck

[11] G. Chikovani, M. N. Focacci, W. Kienzle, C. Lechanoine, B. Lavrat, B. Maglić, M. Martin, P. Schübelin, L. Dubal, M. Fischer, P. Frieder, H. A. Neal, and C. Nef, Phys. Letters **25B**, 44 (1967); D. J. Crennell, U. Karshon, K. W. Lai, J. M. Scarr, and I. O. Skillicorn, Phys. Rev. Letters **20**, 1318 (1968); M. Aguilar-Benitez, J. Barlow, L. D. Jacobs, P. Malecki, L. Montanet, M. Tomaś, M. Della Negra, J. Cohen-Ganouna, B. Lörstad, and N. West, Phys. Letters **29B**, 62 (1969).

[12] J. C. Berlinghieri, M. S. Farber, T. Ferbel, R. Holmes, P. F. Slattery, S. Stone, and H. Yuta, Phys. Rev. Letters **23**, 42 (1969).

[13] N. M. Cason, J. W. Lamsa, N. N. Biswas, I. Derado, T. H. Groves, V. P. Kenney, J. A. Poirier, and W. D. Shephard, Phys. Rev. Letters **18**, 880 (1967); G. Ascoli, H. B. Crawley, U. Kruse, D. W. Mortara, E. Schafer, A. Shapiro, and B. Terreault, *ibid.* **21**, 113 (1968).

[14] B. French, in *Proceedings of the Fourteenth International Conference on High-Energy Physics, Vienna, 1968* (CERN, Geneva, 1968), p. 91.

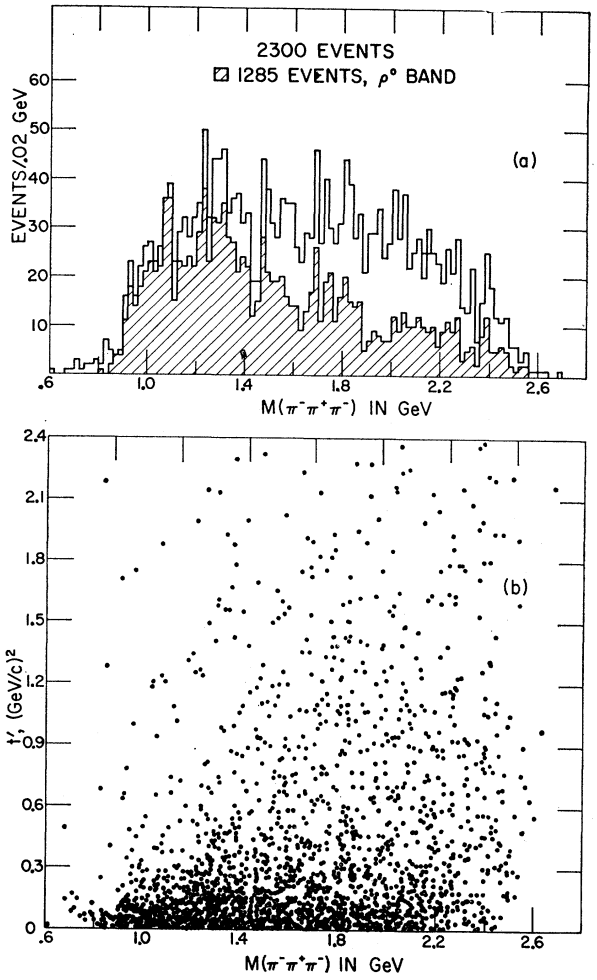

FIG. 11. (a) Effective-mass spectrum of the $\pi^-\pi^+\pi^-$ system. Shaded events are those with at least one $\pi^+\pi^-$ combination in the ρ^0 band. (b) Chew-Low plot for the $\pi^-\pi^+\pi^-$ system.

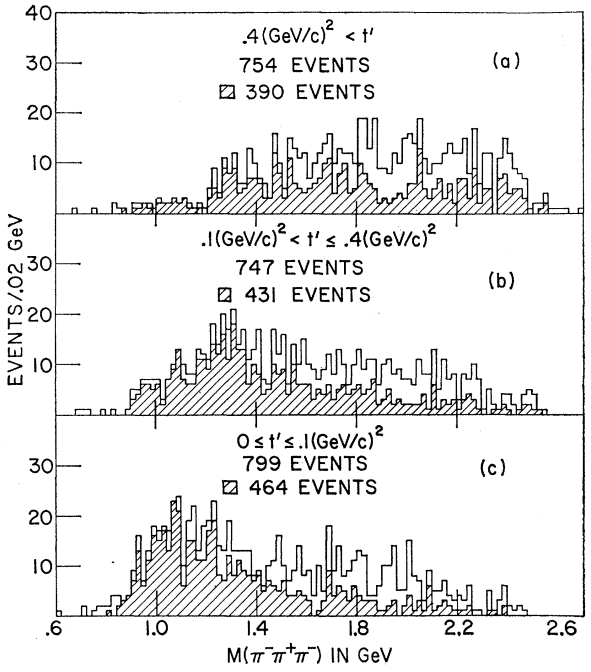

FIG. 12. Effective-mass spectrum of the $\pi^-\pi^+\pi^-$ system as a function of momentum transfer (t'). Shaded events are those with a $\pi^+\pi^-$ combination in the ρ^0 band. (a) 0.4 $(\mathrm{GeV}/c)^2 < t'$. (b) $0.1 < t' \leq 0.4$ $(\mathrm{GeV}/c)^2$. (c) $0 \leq t' \leq 0.1$ $(\mathrm{GeV}/c)^2$.

effect[15] is too broad to match some experimental observations.[16] More recently, models involving Regge-trajectory exchange[8,17] have been applied to three-body final states. These models produce a low-mass enhancement that is narrower than that produced by the usual Deck-type calculation. According to the concept of duality[18] as expressed by Chew and Pignotti,[19] these kinematically predicted enhancements can also be interpreted as including in an average sense the presence of true resonances in the region of the enhancement.

An application of a DRPM to the $\rho^0\pi^- p$ final state can be described by either of the multiperipheral diagrams shown in Fig. 13. Diagrams not involving Pomeranchuk exchange or including baryon exchange have not been considered.

The largest part of the $\rho\pi p$ events are describable by the diagram in Fig. 13(a), since $\sim 80\%$ of these events have the ρ^0 more peripheral than the π^- and the ρ^0 decay distributions shown in Figs. 7(c) and 7(d) are consistent with this choice of diagram. The sample of events with a peripheral ρ^0 is shown in Fig. 14, where $|t_{\pi\rho}|$ is required to be less than 1.0 $(\mathrm{GeV}/c)^2$. In Fig. 14(b) the π^- mesons populate the central region of the Peyrou plot,

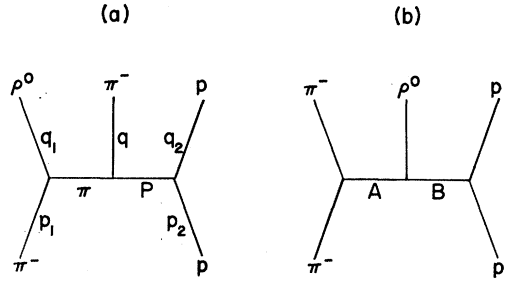

FIG. 13. Multiperipheral diagrams for the $\pi^- p \to \rho^0\pi^- p$ reaction. In (b), A and B can be the ρ and Pomeranchuk trajectories or vice versa.

[15] R. T. Deck, Phys. Rev. Letters **13**, 169 (1964).
[16] E. L. Berger, Phys. Rev. **166**, 1525 (1968).
[17] E. L. Berger, E. Gellert, G. A. Smith, E. Colton, and P. E. Schlein, Phys. Rev. Letters **20**, 964 (1968); M. L. Ioffredo, G. W. Brandenburg, A. E. Brenner, B. Eisenstein, L. Eisenstein, W. H. Johnson, Jr., J. K. Kim, M. E. Law, B. M. Salzberg, J. H. Scharenguivel, L. K. Sisterson, and J. J. Szymanski, *ibid.* **21**, 1212 (1968); G. Alexander, A. Firestone, C. Fu, G. Goldhaber, and A. Pignotti, Phys. Rev. **177**, 2092 (1969); J. G. Rushbrooke and J. R. Williams, Phys. Rev. Letters **22**, 248 (1969); J. Andrews, J. Lach, T. Ludlam, J. Sandweiss, and H. D. Taft, *ibid.* **22**, 731 (1969); S. U. Chung, R. L. Eisner, N. F. Bali, and D. Lüers, Phys. Rev. **182**, 1443 (1969).
[18] R. Dolen, D. Horn, and C. Schmid, Phys. Rev. **166**, 1768 (1968).
[19] G. F. Chew and A. Pignotti, Phys. Rev. Letters **20**, 1078 (1968).

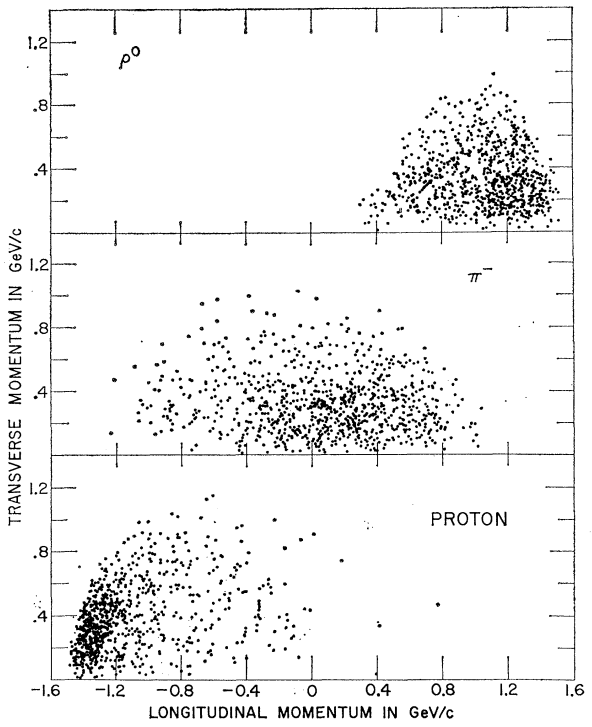

FIG. 14. Longitudinal versus transverse momentum for the particles in the $\pi^- p \to \rho^0 \pi^- p$ reaction selected for a DRPM comparison. The selection of the events shown is described in the text.

while the proton distribution in Fig. 14(c) is peripheral. The selection criteria yield 880 events containing approximately 500 true $\rho\pi p$ events. In 13% of these events, both $\pi^+\pi^-$ mass combinations were in the ρ band and the combination which had its mass closer to 765 MeV was used. The background from non-ρ^0 events was studied in detail by investigating events with a $\pi^+\pi^-$ mass combination immediately adjacent to the ρ^0 band. The distributions discussed here and in the following paragraphs are essentially the same for these events as for those events falling in the ρ^0 band. For this reason, no background subtraction was performed and the diagram in Fig. 13(a) was compared with the full sample of events selected by the criteria above.

The DRPM used is that proposed by Berger[8] and is summarized in the Appendix. Model calculations of the two-body mass plots and the decay angular distributions were accomplished by a Monte Carlo generation of $\rho\pi p$ events at a center-of-momentum energy of 3.5 GeV according to three-body phase space using the program MONTY.[20] These events were then weighted by the matrix elements given in the Appendix and investigated in the same manner as the real events.

The momentum-transfer distributions are shown in Fig. 15, the two-body mass plots in Fig. 16, and the decay angles in Fig. 17. The solid curves in each figure are the predictions of the DRPM, normalized to the number of experimental events. The application of the non-Reggeized Deck-effect one-pion-exchange model (OPEM) is indicated by the dashed curves.

Comparisons of the DRPM and the OPEM indicate that (1) the OPEM has a somewhat better agreement with the experimental $|t_{\pi\pi}|$ distribution shown in Fig. 15(b); (2) the OPEM is in better agreement with the experimental $\pi\rho$ mass distribution shown in Fig. 16(b) (the data do not require the sharp low-mass enhancement as yielded by the DRPM[16]); (3) both models disagree with the experimental πp mass distribution of Fig. 16(c) and the $\pi\rho$ Treiman-Yang distribution of Fig. 17(b); (4) the DRPM has a distinctively better agreement with the πp experimental Treiman-Yang distribution shown in Fig. 17(f). A major fault in the application of both models is that the parametrization of the $\pi^- p$ elastic scattering is inadequate. The $\pi^- p$ elastic differential cross section is normalized to the total $\pi^- p$ cross section via the optical theorem with the implicit assumption that the total cross section is independent of the $\pi^- p$ mass. This, in fact, is not true; the low $\pi^- p$ masses contribute more to the elastic and total cross sections than the high $\pi^- p$ masses. In addition, the DRPM is derived under the assumption of high values of the final-state two-body masses. To examine these effects, the experimental data were required to have $M(\pi^- p) > 1.65$ GeV and comparisons were made with both the DRPM and OPEM including this restriction. This comparison is indicated by the cross-hatched

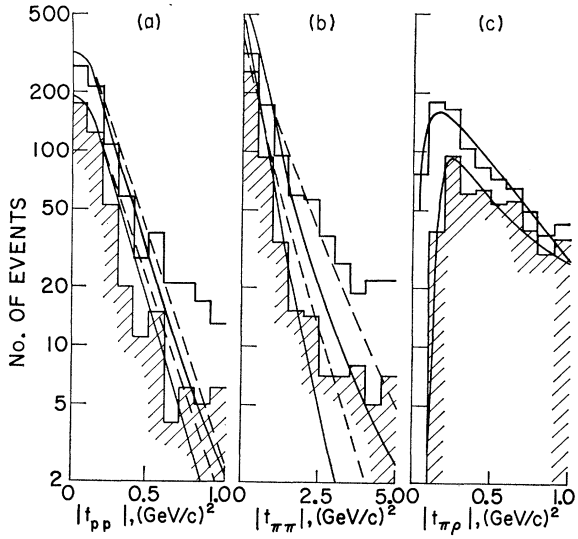

FIG. 15. (a) Experimental distributions for $|t_{pp}|$, the four-momentum transfer squared between target proton and outgoing proton. The solid curve represents the result of the DRPM and the dashed curve that of the OPEM. The shaded histogram and associated curves represent the data and models with $M(\pi^- p) > 1.65$ GeV. (b) and (c) are similar distributions for $|t_{\pi\rho}|$ and $|t_{\pi\pi}|$. In cases where the dashed curve is not shown, it is the same as the solid curve.

[20] J. P. Chandler and C. A. Tilger, Nucl. Instr. Methods **51**, 117 (1967).

histograms and associated curves in Figs. 15–17. The previous conclusions concerning the comparisons of the two models with the data are unchanged with the exception of the distributions for the $\pi^- p$ invariant mass and the $\rho\pi$ Treiman-Yang angle which now show fair agreement between experiment and both models.

Other experimental results have been analyzed by the DRPM with restriction to high values of all invariant two-body masses in the final state.[21] The application of the DRPM including low values of the two-body masses in the present data is indicated by the Dolen-Horn-Schmid duality concept[18] and elucidated for three-body final states by Chew and Pignotti[19] and Berger.[8] In view of this concept, our present results are not inconsistent with a resonance interpretation for the low-mass $\rho\pi$ enhancement.

B. $\pi^-\pi^- p$ Mass Spectrum

The $\pi^-\pi^- p$ invariant-mass spectrum is displayed in Fig. 18. The solid curve shows Lorentz-invariant phase space. Most of the deviation of the experimental distribution from phase space results from kinematic reflections of the $\Delta^{++}(1236)$. The shaded events in the histogram represent events with their $\pi^+ p$ mass in the $\Delta^{++}(1236)$ band. The dashed curve is phase space normalized to the events remaining after removing the $\Delta^{++}(1236)$ band.

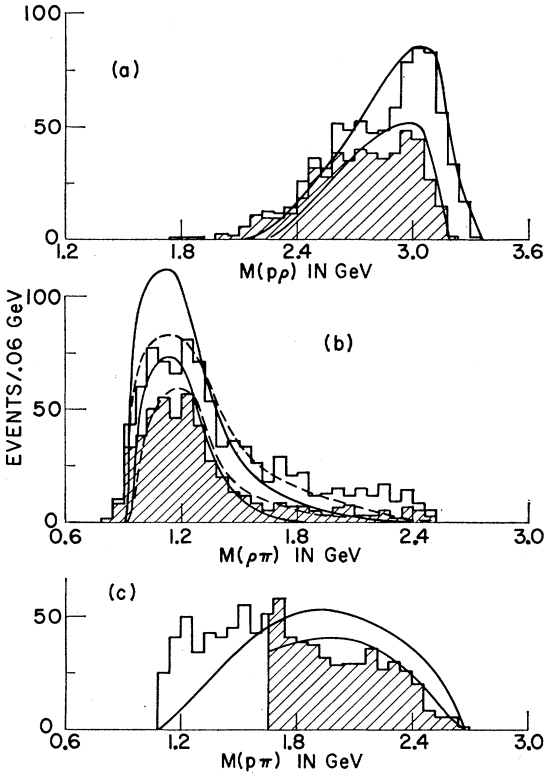

FIG. 16. (a) ρp mass distribution. (b) $\rho\pi$ mass distribution. (c) πp mass distribution. The curves and shaded histograms are explained in the caption for Fig. 15.

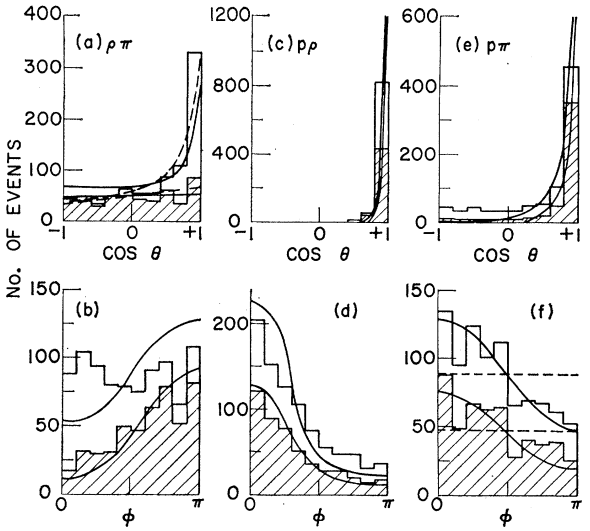

FIG. 17. (a) The Jackson angle for the $\rho\pi$ system defined as $\cos\theta = \mathbf{q}_1 \cdot \mathbf{p}_1 / |\mathbf{q}_1|\,|\mathbf{p}_1|$ in the rest system of the $\rho\pi$ where $\mathbf{q}_1$ and $\mathbf{p}_1$ are the three-momenta of the particles as described in Fig. 13(a). (b) Treiman-Yang angle for the $\rho\pi$ system, defined as $\phi = \cos^{-1}[(\mathbf{p}_1 \times \mathbf{q}_1)/|\mathbf{p}_1 \times \mathbf{q}_1| \cdot (\mathbf{p}_2 \times \mathbf{q}_2)/|\mathbf{p}_2 \times \mathbf{q}_2|]$. (c) and (d) are the Jackson and Treiman-Yang angles for ρp system. (e) and (f) are similar plots for the πp system. Shaded curves and histograms are explained in the caption for Fig. 15.

C. $\pi^+\pi^- p$ Mass Spectrum

Evidence for isobars decaying into $\pi^+\pi^- p$ has been seen in several different final states. The $\pi^+\pi^- p$ effective-mass histogram shown in Fig. 19 deviates noticeably from phase space in the low-mass region. The shaded portion of Fig. 19 represents events with the $\pi^+ p$ mass in the Δ^{++} band.

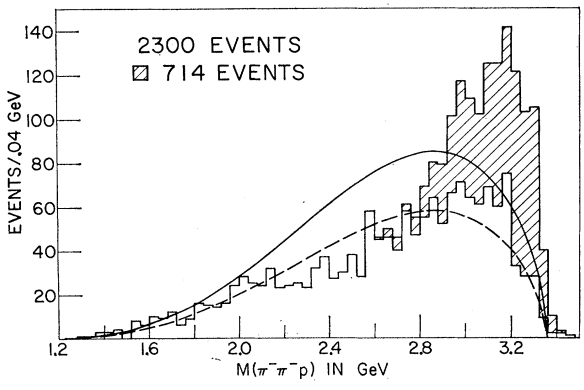

FIG. 18. Effective mass of the $\pi^-\pi^- p$ system. Shaded events have their $\pi^+ p$ mass in the $\Delta^{++}(1236)$ band. The solid curve is phase-space normalized to 2300 events. The dashed curve is normalized to the distribution with the Δ^{++} events removed.

[21] C. Hong-Mo, K. Kajantie, and G. Ranft, Nuovo Cimento **49A**, 157 (1967); C. Hong-Mo, K. Kajantie, G. Ranft, W. Beusch, and E. Flaminio, *ibid.* **51A**, 696 (1967).

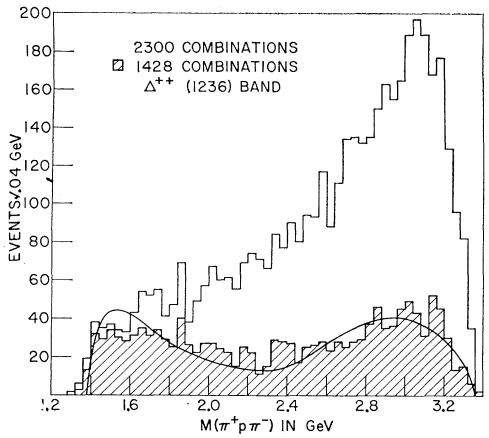

FIG. 19. Effective mass of the $\pi^+\pi^-p$ system. Shaded events have the π^+p effective mass in the $\Delta^{++}(1236)$ band. The solid curve is the result of a DRPM calculation for the $\Delta^{++}\pi^-$ distribution.

We have applied the DRPM to the $\Delta^{++}\pi^-\pi^-$ final state. The data are in good agreement with the predictions of the model. The details of the calculation and the comparisons with the data are given in Ref. 10. The DRPM calculation of the $\Delta^{++}\pi^-$ mass spectrum is included as the solid curve in Fig. 19 and shows a low-mass enhancement.

We have also observed and reported evidence for a 1700-MeV enhancement in the $\pi^+\pi^-p$ mass spectrum.[22] The enhancement is associated with a subset of events having high momentum transfer to the final-state proton. Our best estimates of the mass and width are 1730 ± 18 and 55 ± 15 MeV, respectively. Other production experiments have seen evidence for an isobar near 1700 MeV with $N\pi\pi$ decay modes and a narrow width.[23] Our values of the mass and width are consistent with these observations.

ACKNOWLEDGMENTS

The authors would like to thank Professor Ray R. Crittenden, Dr. T. M. Small, and Dr. K. F. Suen for their contributions in the early stages of this experiment. We would like to express our gratitude to our scanning and measuring staff at Indiana University and to the zero-gradient synchrotron operating staff and the crew of the 30-in. bubble chamber at the Argonne National Laboratory for their aid during this exposure.

APPENDIX

The multiperipheral Regge-pole model proposed by Berger[8] has been applied to the diagram shown in Fig. 13(a). The square of the matrix element averaged over initial spins and summed over final spins is given by

$$\sum|M|^2_{\mathrm{DRPM}}=\frac{(\pi\alpha_\pi')^2N}{2(1-\cos\pi\alpha_\pi)}[S_0^{-1}(S_1\cdots)]^{2\alpha_\pi}\times(S_2\cdots)^2e^{at_2},$$

where

$$S_1\cdots=S_1-t_2-m_\pi^2+\tfrac{1}{2}t_1^{-1}(m_\rho^2-m_\pi^2-t_1)(m_\pi^2-t_1-t_2),$$
$$S_2\cdots=S_2-t_1-m_p^2-\tfrac{1}{2}(m_\pi^2-t_1-t_2),$$
$$S_i=(q+q_i)^2,\quad t_i=(p_i-q_i)^2,\quad \alpha_\pi=(t_1-m_\pi^2)\alpha_\pi',$$
$$N=g_\rho^2\sigma^2_{\mathrm{tot}}(\pi^-p).$$

The parameter a was chosen as 5.0 $(\mathrm{GeV}/c)^{-2}$ to give agreement between the model and the experimental t_{pp} distribution shown in Fig. 15(a). The Pomeranchuk trajectory has $\alpha_p=1.0$ and has been modified by exponential damping. The parameters S_0 and α_π' were chosen as 0.8 and 1.0 GeV^2, respectively, and gave good agreement with the experimental $t_{\pi p}$ distribution shown in Fig. 15(b). The same or similar values of S_0 and α_π' describe the data in other reactions at widely differing momenta.[17]

The normalization constant, $N=g_\rho^2\sigma^2_{\mathrm{tot}}(\pi^-p)$, in the DRPM is chosen so that it agrees with a Deck-type OPEM in the limit $t_1\to m_\pi^2$. The OPEM matrix element squared is

$$\sum|M|^2_{\mathrm{OPEM}}=\frac{g_\rho^2\sigma^2_{\mathrm{tot}}(\pi^-p)[S_2-(m_\pi-m_p)^2][S_2-(m_\pi+m_p)^2]e^{at_2}}{(t_1-m_\pi^2)^2}.$$

The OPEM is normalized to $\sigma_{\mathrm{tot}}(\pi^-p)$ using the optical theorem assuming no real part of the πp forward-scattering amplitude. The theoretical cross section is given by

$$d\sigma=\frac{1}{(2\pi)^5}\frac{1}{4F}\sum|M|^2d\Phi_3,$$

where $F=m_p\times p_{\mathrm{inc}}$ and $d\Phi_3$ is the three-body invariant phase space. Using 120 MeV as the width of the ρ^0 and 36 μb [24] for $\sigma_{\mathrm{tot}}(\pi^-p)$, the DRPM with our choice of S_0 and α_π' predicts a cross section of 325 μb for the $\rho\pi p$ final state. Experimentally, we observe 600 μb.

[22] K. F. Galloway, E. D. Alyea, Jr., R. R. Crittenden, W. F. Prickett, and H. J. Martin, Jr., Phys. Letters **27B**, 250 (1968).

[23] P. Fleury, J. Huc, R. Vanderhaghen, J. Duboc, R. George, M. Goldberg, V. Picciarelli, A. Romano, and A. Quareni-Vignudelli, Phys. Letters **26B**, 686 (1968); S. Miyashita, J. von Krogh, J. B. Kopelman, and L. Marshall Libby, Nuovo Cimento (to be published).

[24] The π^-p total cross sections [see G. Källén, *Elementary Particle Physics* (Addison-Wesley, Reading, Mass., 1964)] have been averaged over the present theoretical π^-p mass spectrum.